Structure−Function Relationship of the Fifth Transmembrane Domain in the Na^+/H^+ Antiporter of *Helicobacter pylori*: Topology and Function of the Residues, Including Two Consecutive Essential Aspartate Residues†

Naoyuki Kuwabara, Hiroki Inoue, Yumi Tsuboi, Keiji Mitsui, Masafumi Matsushita, and Hiroshi Kanazawa*

Biological Sciences, Osaka University, Graduate School of Science, 1-16 Machikaneyama-cho 1-1, Toyonaka City, Osaka 560-0043, Japan

Received May 26, 2006; Revised Manuscript Received September 23, 2006

ABSTRACT: We examined the structure−function relationships of residues in the fifth transmembrane domain (TM5) of the Na^+/H^+ antiporter A (NhaA) from *Helicobacter pylori* (HP NhaA) by cysteine scanning mutagenesis. TM5 contains two aspartate residues, Asp-171 and Asp-172, which are essential for antiporter activity. Thirty-five residues spanning the putative TM5 and adjacent loop regions were replaced by cysteines. Cysteines replacing Val-162, Ile-165, and Asp-172 were labeled with NEM, suggesting that these three residues are exposed to a hydrophilic cavity within the membrane. Other residues in the putative TM domain, including Asp-171, were not labeled. Inhibition of NEM labeling by the membrane impermeable reagent AMS suggests that Val-162 and Ile-165 are exposed to a water filled channel open to the cytoplasmic space, whereas Asp-172 is exposed to the periplasmic space. D171C and D172C mutants completely lost Na^+/H^+ and Li^+/H^+ antiporter activities, whereas other Cys replacements did not result in a significant loss of these activities. These results suggest that Asp-171 and Asp-172 and the surrounding residues of TM5 provide an essential structure for H^+ binding and Na^+ or Li^+ exchange. A168C and Y183C showed markedly decreased antiporter activities at acidic pH, whereas their activities were higher at alkaline pH, suggesting that the conformation of TM5 also plays a crucial role in the HP NhaA-specific acidic pH antiporter activity.

Sodium proton antiporters are ubiquitous membrane proteins found in the plasma membrane and organelle membranes of cells from various origins, including plants, animals, and microorganisms (*1*−*5*). These antiporters play a primary role in the regulation of intracellular pH and cellular Na^+ concentrations by exchanging Na^+ for H^+. In *Escherichia coli*, three Na^+/H^+ antiporters (EC NhaA[1], NhaB, and ChaA) are known (*1*), and their functional characteristics have been well described (*5*−*9*). Among the three antiporters, EC NhaA plays a major role in regulating intracellular Na^+ concentrations (*1*). The activity of EC NhaA is dependent on environmental pH and increases markedly as pH is elevated from neutral to alkaline; at pH 7.0, EC NhaA has a negligible antiporter activity, whereas at pH 8.5, it is enhanced by 3 orders of magnitude (*8*). The topological arrangement of 12 putative transmembrane helices (TM) in EC NhaA has been modeled on the basis of its hydropathy profile and its secondary structure, as revealed by *pho*A fusion experiments (*10*), as well as on the basis of its tertiary structure, elucidated by crystallographic analysis at 7 Å resolution (*11*). For EC NhaA, three Asp residues in the fourth and the fifth TMs (TM4 and 5) are essential for ion transport (*12*), whereas His-225 (*13*, *14*) and Gly-338 (*15*) play important roles in pH sensing. Although extensive studies have been performed, the structure−function relationships integrating the mechanisms of ion transport and pH sensing are not fully understood.

We have previously shown that NhaA from *H. pylori* (HP NhaA) functions in *E. coli* and exhibits a profile of pH dependent antiporter activity very different from that of EC NhaA (*16*). HP NhaA is constitutively active from weakly acidic to alkaline pH (pH 6.0 to 8.5), in contrast to EC NhaA, even though the two proteins have extensive homology at the primary sequence level. We have analyzed the molecular basis underlying this difference in pH sensitivity between HP and EC NhaA in an effort to elucidate the mechanisms of pH sensing by antiporters (*12*, *13*, *16*−*19*). Chimeric and random-mutational analyses have shown that the difference is not determined by the unique sequence found in the loop structure between TM8 and 9 (loop8) of HP NhaA but by TM4, 5, and 10, which are highly conserved between the two NhaAs (*17*, *18*). Moreover, mutations causing severe reduction of activity at any pH range have been mapped to two distant regions in the primary sequence, TM4−5 and TM10−11 (*18*). These results suggest that TM4, 5, 10, and 11 together constitute the essential components of the ion transport pathway (*18*). In our previous study, we conducted cysteine scanning mutagenesis of TM4 and analyzed altered

† This study was supported by a Grant-in-Aid for scientific research from the Ministry of Education, Science, Culture, Sports and Technology of Japan.

* Corresponding author. Tel: 06-6850-5812. Fax: 06-6850-5812. E-mail: kanazawa@bio.sci.osaka-u.ac.jp.

[1] Abbreviations: NhaA, Na^+/H^+ antiporter; EC NhaA, *E.coli* NhaA; HP NhaA, *H.pylori* NhaA; TM, transmembrane domain; NEM, *N*-ethylmaleimide; AMS, 4-acetamide-4′-maleiimidylstilbene-2,2′-disulfonic acid.

10.1021/bi061048d CCC: $33.50
Published on Web 11/15/2006

antiporter activity in the mutants (*19*). These results indicated that TM4 faces an aqueous environment and that Thr-140 and Asp-141 may form a Na^+ or Li^+ binding site.

Recently, the crystal structure of EC NhaA at 3.4 Å was reported (*20*). The crystal structure clearly showed the presence of a negatively charged ion funnel-like structure, which is open to the cytoplasm and terminates in the middle of the membrane at a putative ion binding site. Because the crystals were grown at pH 4, the structure represents the inactive state of NhaA. Thus, the active state structure is not unknown. To reveal the ion transport mechanism of NhaA, it is essential to analyze the structure of the active form of NhaA. In this study, to survey residues involved in the antiport mechanism including its pH dependency, we performed scanning cysteine substitution and chemical modification by NEM of residues within TM5 together with the neighboring loop regions of HP NhaA. The NEM binding assay is applicable only to neutral pH conditions, and HP NhaA is fully active at pH 7, whereas EC NhaA is not. Therefore, the Cys scanning mutagenesis and subsequent assays are only applicable to the structure of HP NhaA (*21*).

Twenty-three residues between Leu-160 and Phe-182 were in a hydrophobic membrane domain, but some residues within this region (Val-162, Ile-165, and Asp-172), residing on one side of a putative α-helix, are located in a hydrophilic environment, possibly facing a water filled ion transport channel. These results are consistent with the crystal structure of EC NhaA and provide important structural and functional insights into the ion transport mechanism of HP NhaA.

MATERIALS AND METHODS

Materials and Reagents. Restriction endonucleases, T4 DNA ligase, and KOD DNA polymerases were purchased from TOYOBO (Osaka, Japan), and LA-Taq polymerase was purchased from TaKaRa Bio, Inc. (Shiga, Japan). Oligonucleotides were synthesized by Invitrogen (Carlsbad, CA). *N*-[ethyl-1-^{14}C]maleimide ([^{14}C]NEM, 1.3 GBq/mmol) was purchased from NEN Life Science Products (Boston, MA). Other reagents and materials were of the highest commercially available grade.

Bacterial Strains and Culture Conditions. The *E. coli* strain KNabc (Δ*nha*A::Km^r, Δ*nha*B::Em^r, Δ*cha*A::*Cm*^{r}, *sup*E, *hsd*Δ5, *thi*, Δ (*lac-pro*AB)/F′ (*tra*Δ36, *pro*AB$^+$, *lac*I^q, *lac*ΔM15)) (*22*, *23*) was used to express HP NhaA mutant proteins and construct various plasmids, respectively. Cells were cultured in L broth (LB) (*24*) containing 87 mM KCl instead of NaCl (LBK). For growth on solid plates, agar, (1.5% w/v) was added to the medium. Transformants were selected using an appropriate antibiotic. For analysis of salt tolerance in KNabc transformed with various plasmids, various concentrations of NaCl or LiCl were added to LB plates containing 87 mM NaCl. The plates and broth cultures were incubated at 37 °C.

Construction of Expression Plasmids. The construction of HP NhaA expression plasmids derived from pBR322 has been described previously (*16*). HP NhaA with a FLAG epitope tag at the 3′ end of the coding region was expressed from these plasmids under the control of the *tet* promoter. NhaAs expressed from these vectors contain an additional sequence, GMQ, at the junction of the FLAG tag sequence (DYKDDDDK).

Site-Directed Mutagenesis. Site-directed mutations were introduced using the two-step PCR method (*25*) or the oligodeoxyribonucleotide-directed dual amber (ODA) method (*26*). Cys-less HP *nha*A was constructed in the previous study (*19*) and was used to replace residues with Cys. DNA fragments encoding Cys-less HP NhaA were cloned into pBR-HP instead of native HP NhaA. pKF19k, harboring the FLAG-tagged Cys-less HP NhaA gene, was used as a DNA template for ODA mutagenesis. DNA fragments encoding HP NhaA, in which a single cysteine had been introduced, were ligated back into the corresponding sites of pBR-HP. The DNA sequences of all mutagenized *nha*A were verified by DNA sequencing.

Immunological Detection of FLAG-Tagged NhaAs. The expression of HP NhaA and mutated HP NhaA was detected by western blot analysis, as described previously (*17*, *27*).

Preparation of Membrane Vesicles, and Na^+/H^+ and Li^+/H^+ Antiporter Assays. Everted membrane vesicles from *E. coli* cells, which had been transformed with various expression plasmids, were prepared and used to determine Na^+/H^+ or Li^+/H^+ antiporter activity, as described previously (*28*−*30*). Everted membrane vesicles (100 μg) were resuspended in 2 mL of assay buffer (10 mM Tricine and 140 mM KCl, adjusted to the desired pH with KOH). Proton flow was measured by monitoring fluorescence quenching of 9-amino-6-chloro-2-methoxyacridine (ACMA) after the addition of potassium lactate (5 mM, pH 7.0), a substrate of the electron transport respiratory chain. Fluorescence dequenching after the addition of 5 mM NaCl or LiCl was monitored with a fluorimeter (JASCO FP-750, JASCO Ltd., Tokyo Japan) to measure antiporter activity. As shown previously, the end level of dequenching is a good estimate of antiporter activity (*31*).

[^{14}C]NEM Modification. The [^{14}C]NEM binding experiment was performed using sonicated membranes prepared from *E. coli* KNabc cells expressing Cys-less NhaA or single cysteine mutants. Sonicated membranes (0.5 mg protein) were incubated in 100 μL of 50 mM MOPS−KOH buffer (pH 7.0) containing 0.1 M KCl and 0.5 mM [^{14}C]NEM (Perkin-Elmer Life Sciences) at 30 °C for 5 min. The modification reaction was stopped by adding 100 μL of 20 mM unlabeled NEM to the reaction mixture, followed by ultracentrifugation at 200,000*g* for 1 h at 2 °C. The resultant precipitate was resuspended in 200 μL of 10 mM sodium phosphate buffer (pH 7.4) containing 0.1 M NaCl and 1% Triton X-100. The suspension was centrifuged at 178,000*g* for 30 min with an Airfuge (Beckman) to remove insoluble substances. The resultant supernatant was subjected to immunoprecipitation with anti-FLAG M2 monoclonal antibodies conjugated to agarose beads (Sigma, St. Louis, MO). Immunoprecipitates were solubilized in 15 μL of 0.125 M Tris-HC1 buffer (pH 6.8) containing 4% SDS, 20% glycerol, and 0.004% bromophenol blue. SDS−PAGE was performed with the solubilized aliquot, according to the method of Laemmli (*32*). The ^{14}C-labeled NhaA protein was visualized and quantified using a BAS2500 bio-imaging system (Fuji Film, Tokyo, Japan).

Prevention of [^{14}C]NEM Binding by 4-Acetamido-4′-maleimidylstilbene-2-2′-disulfonic Acid (AMS) or Silver Ions. In these assays, 5 μL of 100 mM AMS (final concentration, 5 mM), 5 μL of 10 mM $AgNO_3$ (final concentration, 0.5 mM), or an equivalent volume of distilled water was added

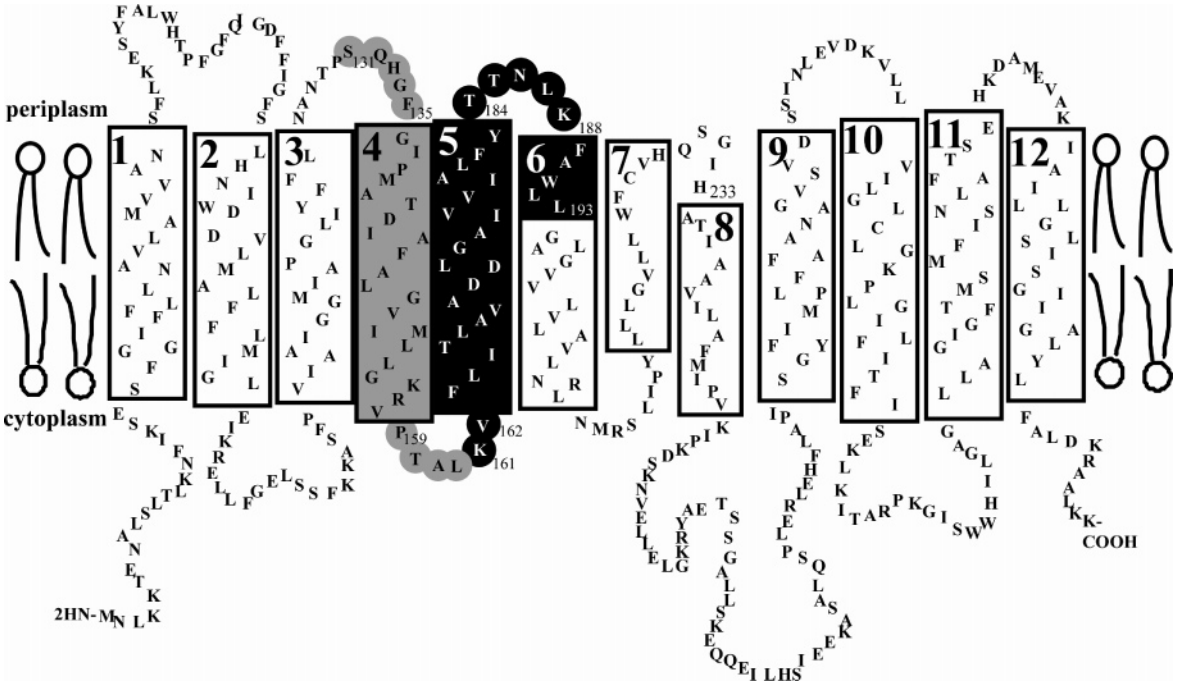

FIGURE 1: Secondary structure model of HP NhaA predicted by hydropathy analysis (*16*) and our previous study (shaded in gray) (*19*). The residues substituted to cysteine in TM5, loop4, loop5, and TM6 (Lys-161 to Leu-192) are shown in white on a black background. The native cysteine residues (Cys-226 in TM7 and Cys-344 in TM10) were substituted to serine in the Cys-less HP NhaA.

to 100 μL of a suspension of intact *E. coli* KNabc cells expressing mutant NhaA or to a sonicated membrane suspension containing a mutant NhaA, followed by incubation for 30 min at 30 °C. Subsequently, 20 μL of 3 mM [^{14}C]NEM (final concentration, 0.5 mM) was added to the reaction mixture, followed by incubation for 30 min, and then the mixture was diluted with 900 μL of the same buffer containing 5 mM unlabeled NEM. *E. coli* cells were collected and washed once with the same buffer immediately after dilution and then were disrupted by brief sonication. The membranes were collected by ultracentrifugation and solubilized, and NhaA proteins were immunoprecipitated, as described above. The intensities of radioactive bands following pretreatment with AMS or Ag^+ were compared to those without treatment. To prevent AgCl precipitation, KNO_3 was added to all buffers instead of KCl.

DNA Manipulation and Other Procedures. Preparation of plasmids, digestion by restriction endonucleases, ligation of the DNA fragments by T4 DNA ligase, and other techniques related to DNA handling were performed according to published procedures (*33*). The nucleotide sequences of DNA fragments cloned into the various expression plasmids in this study were determined using an automated DNA sequencer (Model 377; Applied Biosystems, Foster City, CA). Protein concentration was determined by the Lowry method using bovine serum albumin as a standard (*34*).

RESULTS

Antiporter Activity of Single Cysteine Mutants of HP NhaA. To replace residues in TM5 and flanking regions (Figure 1) with cysteines, we used a Cys-less HP NhaA mutant in which both of the two native cysteine residues were changed to serine residues without decreasing antiporter activity (*19*). We first measured the amount of NhaA protein by western blot analysis of the total membrane preparations (Figure 2A). The expression levels of the mutant NhaA proteins in the membrane preparation were detected using antibodies against the FLAG tag, which was fused to the *C*-termini of the mutants. All of the mutant NhaAs, with the exception of V162C, were present in the membrane in amounts comparable to that of the wild type. Therefore, the differences in antiporter activity between Cys-less and cyteine mutants, with the exception of V162C, cannot be attributed to their defective insertion into the membrane. The Na^+/H^+ antiporter activity of each cysteine NhaA mutant was assessed using everted membrane vesicles prepared from *E. coli* KNabc cells expressing a single cysteine mutant NhaA. The activity was tested at pH 7.5 in the presence of 5 mM NaCl, conditions that supported maximal activity for both the wild type and Cys-less HP NhaA. Although the antiporter activities of most of the mutants (28 of 33) were similar to that of the Cys-less HP NhaA, A168C, D171C, D172C, and Y183C NhaA, antiporter activities were significantly lower than that of Cys-less HP NhaA (Figure 2B). No activity was observed in the D171C and D172C mutants, which is consistent with previous results, suggesting that two Asp residues of the EC NhaA corresponding to these HP NhaA residues are part of an ion binding site in the antiport mechanism (*12*). To assess the role of Ala-168 and Tyr-183 in the anitiporter mechanism, we analyzed kinetic parameters for these mutants (Table 1). The apparent K_m for Na^+ increased 11- and 14. 5-fold in the A168C and Y183C mutants, respectively, whereas the apparent K_m for Li^+ also increased 2.6- and 7.3-fold in the A168C and Y183C mutants, respectively. The V_{max} values were similar to that of Cys-less HP NhaA. These increases in K_m values suggest that Ala-168 and Tyr-183 play an important role in the antiport mechanism. The different degrees in the changes of K_m between Na^+ and Li^+ might be due to the difference in the structures involved in Na^+ and Li^+ binding suggested previously (*17*, *19*, *39*).

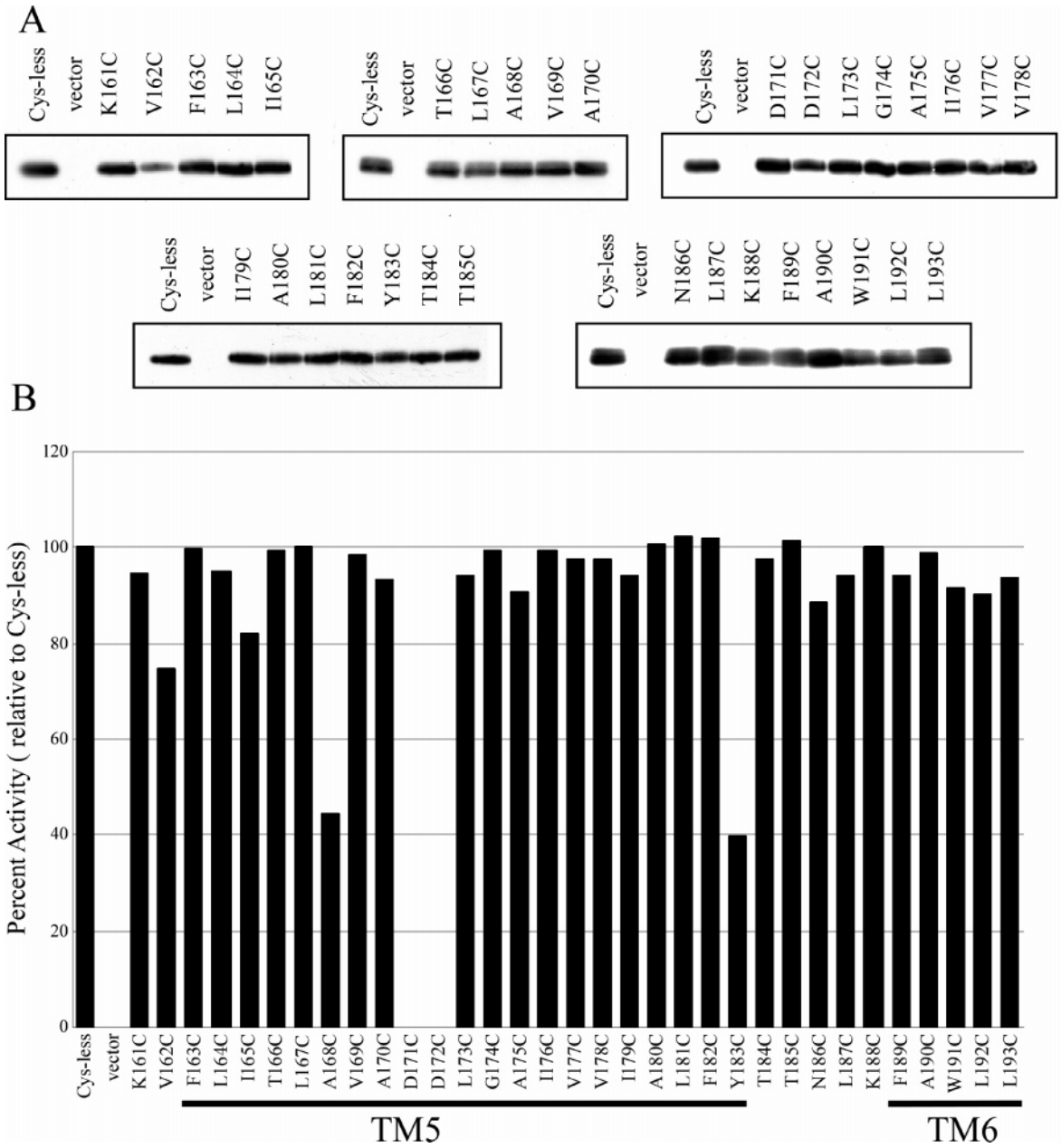

FIGURE 2: Expression and transporter activity of Cys-less and cysteine mutant NhaAs. (A) Membrane proteins (1.5 μg total protein) from the KNabc strain transformed with a plasmid expressing a FLAG-tagged Cys-less NhaA or single cysteine mutant NhaAs were subjected to SDS−PAGE (12.5% acrylamide). As a negative control, membrane proteins of cells transformed with pBR322 alone were also analyzed. After electrophoresis, the proteins were transferred to a GVHP membrane and probed with the anti-FLAG monoclonal antibody M2 (Sigma), followed by incubation with horseradish peroxidase-linked anti-mouse IgG. Immunoreactive bands were visualized using ECL (Amersham Biosciences). (B) Everted membrane vesicles were prepared from *E. coli* KNabc transformed by plasmids expressing Cys-less HP NhaA or various Cys-substituted mutants. The Na^+/H^+ antiporter activities at pH 7.5 were determined as described in the Materials and Methods section. The graph shows percent activity, measured as fluorescence dequenching, relative to that of the Cys-less parent mutant.

Labeling of Introduced Cysteines with [^{14}C]NEM. To examine the accessibility of the residues in TM5 and adjacent loops to a hydrophilic environment, we assessed the labeling of each cysteine residue in the cysteine-scanning mutant NhaA series with [^{14}C]NEM (Figure 3). Because maleimide reagents including NEM react with the deprotonated form of sulfhydryl groups and the reaction requires a water molecule as a proton acceptor (*35*−*37*), this procedure can be used for the topological definition of residues in the membrane domain. On the basis of the hydropathy analysis (*16*), the membrane insertion of TM5 was predicted to be between Phe-163 and Tyr-183 (Figure 1). With the exception of three Cys mutants (V162C, I165C, and D172C), Cys mutants between Lys-161 and Phe-182 exhibited very low reactivity to NEM. In addition, on the basis of our previous results (*19*), we predicted that loop 4 (between TM4 and TM5) extended to Ala-159. Thus, TM5 begins with Leu-160 and ends with Phe-182, suggesting that the integral membrane portion is composed of 23 residues (Figure 4A). The NEM labeling experiments indicated that V162C and D172C were highly reactive (Figure 3), whereas I165C exhibited lower reactivity. When these residues are superimposed on an α-helical wheel model and the α helix of TM5 in the EC NhaA crystal structure (Figure 4A and B),

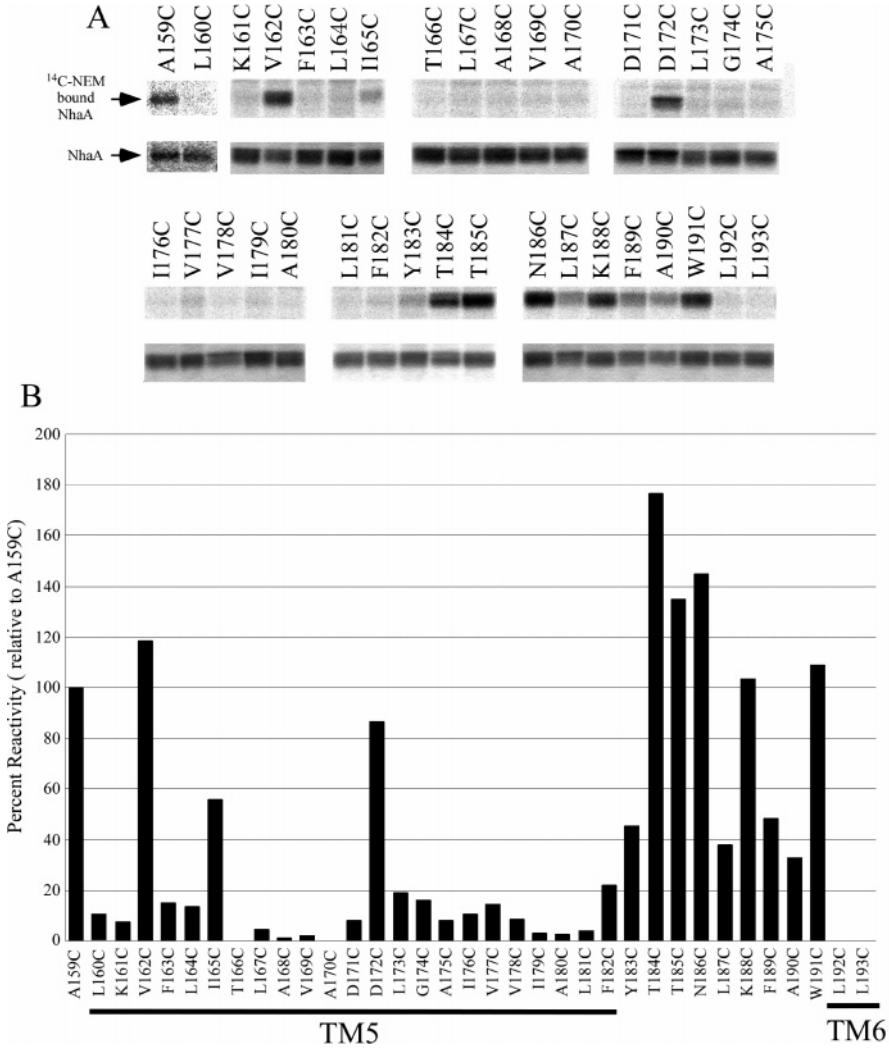

FIGURE 3: [^{14}C]NEM modification identifies residues exposed to a hydrophilic environment. Sonicated membranes (0.5 μg protein) of *E. coli* cells expressing the cysteine scanning mutants were incubated with 0.5 mM [^{14}C]NEM for 5 min at 30 °C, followed by solubilization and immunoprecipitation of NhaA using an anti-FLAG M2-agarose beads (Sigma). The protein bands were visualized after SDS−PAGE as described in Materials and Methods. (A) Radioactive NhaA bands visualized with a BAS-2500 Bioimaging Analyzer (Fujifilm) (upper panels) and the NhaA protein bands visualized by Coomassie Brilliant Blue staining (lower panels). (B) Relative amount of [^{14}C]NEM binding calculated from the band intensities in A. The [^{14}C]NEM binding was normalized to that of the A159C mutant, whose mutation is located in a hydrophilic loop region (Figure 1). TM5 and TM6 shown at the bottom are based on NEM labeling results.

Table 1: Apparent Kinetic Parameters of Cys-Less, A168C, D171C, D172C, and Y183C Mutant NhaA[a]

	Na^+		Li^+	
	K_m (mM)	V_{max} (% dequenching)	K_m (mM)	V_{max} (% dequenching)
Cys-less	0.4 ± 0.2	99 ± 1	0.07 ± 0.01	77 ± 9
A168C	4.5 ± 0.1	71 ± 6	0.18 ± 0.01	85 ± 5
D171C	[b]	[b]	[b]	[b]
D172C	[b]	[b]	[b]	[b]
Y183C	5.8 ± 2.4	74 ± 6	0.51 ± 0.05	55 ± 22

[a] Na^+/H^+ and Li^+/H^+ antiporter activities were measured for the everted membrane vesicles prepared from KNabc cells expressing Cys-less or the indicated mutant NhaA in the presence of various concentrations of NaCl (0.05−50 mM) or LiCl (0.005−5 mM) at pH 7.5. The K_m and V_{max} values were calculated by the linear regression of Lineweaver−Burk plots. The data represent the average of two independent experiments. [b] These values could not be determined because of very little activity.

the residues all reside on one side of the helix. Thus, Val-162, Ile-165, and Asp-172 are likely to be on one side of a putative α-helix, and this side may face a water-filled cavity.

Inhibition of [^{14}C]NEM Labeling by Membrane Impermeable Thiol-Reactive Reagents. To identify whether a putative cavity facing TM5 is open to the cytoplasm or the periplasm, we analyzed the effect of a membrane-impermeable maleimide derivative, 4-acetamide-4′-maleiimidylstilbene-2,2′-disulfonic acid (AMS), on [^{14}C]NEM binding using both intact cells and sonicated membranes. For intact cells expressing a single cysteine NhaA mutant, pretreatment with AMS was predicted to only block the binding of NEM to cysteine residues that are accessibly from the periplasmic side, not the cytoplamic side (*37*). Y183C and T184C were not labeled by NEM when cells were pretreated with AMS (Figure 5), indicating that these residues reside in the periplasmic loop (loop5) (Figure 1). In contrast, the labeling of A159C (loop 4), V162C, I165C, and D172C by NEM in intact cells was not significantly reduced by AMS, indicating that these residues are not exposed to the periplasmic space but probably face the cytoplasmic compartment. However, it is also possible that these residues could be exposed to an occluded aqueous compartment not accessible from either

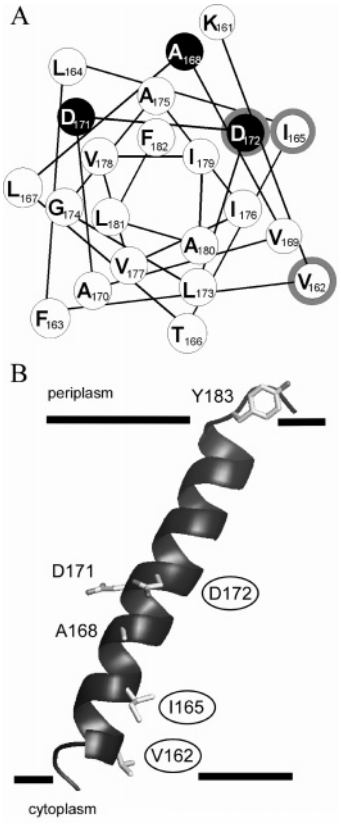

FIGURE 4: (A) Helical wheel projection of TM5, viewed from the cytoplasmic side. The residues of cysteine mutants that showed NEM reactivity, as shown in Figure 3, are outlined in gray. Cys mutants that showed lower activities (shown in Figure 2) are shown with white lettering on a black background. (B) Model of TM5 structure, generated by homology modeling based on the X-ray crystal structure of EC NhaA (pdb code, 1ZCD), showing functionally important residues (Ala-168, Asp-171, Asp-172, and Tyr-183) and the residues located in the hydrophilic environment (circled residues) (*42*). Solid black lines represent the boundary of the membrane indicated by [^{14}C]NEM binding experiments (Figure 3).

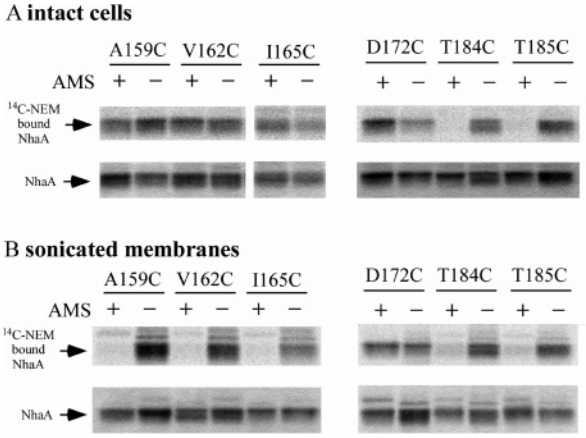

FIGURE 5: Effects of AMS on [^{14}C]NEM binding to the cysteine mutant NhaA proteins in intact cells (A) and in sonicated membranes (B). For both A and B, the upper panels show the radioactive bands on SDS−PAGE gels, and the lower panels show the Coomassie Brilliant Blue staining of NhaA. (A) Intact cells expressing the cysteine mutants were preincubated in the presence (+) or absence (−) of 5 mM AMS for 30 min at 30 °C, followed by incubation with 0.5 mM [^{14}C]NEM for 30 min. After labeling was stopped by diluting in excess unlabeled NEM, the cells were disrupted by brief sonication. The membrane fractions were solubilized, and the NhaA proteins were immunoprecipitated. (B) Sonicated membranes were preincubated in the presence (+) or absence (−) of AMS followed by labeling with [^{14}C]NEM. The membranes were solubilized and NhaA immunoprecipitated, as described above.

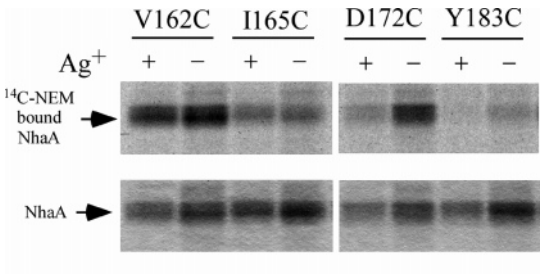

FIGURE 6: Effect of silver ions on [^{14}C]NEM binding to the cysteine mutant NhaA proteins in intact cells. Intact cells expressing the cysteine mutants were preincubated in the presence (+) or absence (−) of 0.5 mM $AgNO_3$ for 30 min at 30 °C, followed by incubation with 0.5 mM [^{14}C]NEM for 30 min. After labeling was stopped by dilution with excess unlabeled NEM, the cells were disrupted by brief sonication. The membrane fraction was solubilized, and NhaA was immunoprecipitated. The radioactive bands on SDS−PAGE gels were visualized as described in Figure 3A.

surface. In sonicated membranes prepared from cells expressing each of these mutant NhaAs, AMS pretreatment blocked NEM labeling of A159C, V162C, I165C, T184C, and T185C (Figure 5). Because sidedness of the membranes is not maintained in the sonicated membranes, AMS is able to access cysteine residues from both sides of the lipid bilayer. Therefore, the result is consistent with the intact cell results, with the exception of D172C.

Interestingly, NEM labeling of D172C NhaA in the sonicated membranes was not blocked in the presence of AMS (Figure 5B), implying that Asp-172 may be embedded in a narrow pocket on the surface of the putative water filled cavity and is accessible to NEM but not to AMS. Because Asp-172 is one of the essential residues for ion transport in NhaA, it is very important to know whether the aspartate residue is accessible from the periplasmic side or not. The inhibition of [^{14}C]NEM modification of D172C in intact cells was further tested, using silver ions that are membrane impermeable but much smaller than AMS to block [^{14}C]NEM binding. To our surprise, NEM binding of D172C was prevented by silver ions in intact cells (Figure 6). These results indicate that Asp-172 is indeed accessible from the periplasmic side.

pH Dependence of the Antiporter Activity of Mutant NhaA. NhaA homologues found in other bacteria, including *E. coli* and *V. parahemeolyticus*, are activated by alkaline pH in the cytoplasm (*8*, *38*). HP NhaA, however, is fully active at acidic pH as well as at alkaline pH. In our previous article (*18*), we proposed that HP NhaA has two activation mechanisms, one active at acidic pH and another active at alkaline pH, similar to that of EC NhaA. To identify mutations that affect the pH dependence of the antiporter activity, we surveyed the antiporter activities of all 35 cysteine mutants under different pH conditions. Most of the mutations, including I165C, did not affect the pH dependency of antiporter activities. As expected, D171C and D172C showed no activity at any pH. The Na^+/H^+ antiporter activities of the A168C and Y183C mutants were remarkably reduced at acidic pH. The pH profiles of Y183C and A168C are similar to that of EC NhaA, which is only active at alkaline pH (Figure 7) Thus, we concluded that Ala-168 and Tyr-183 are involved in an activation mechanism of Na^+/

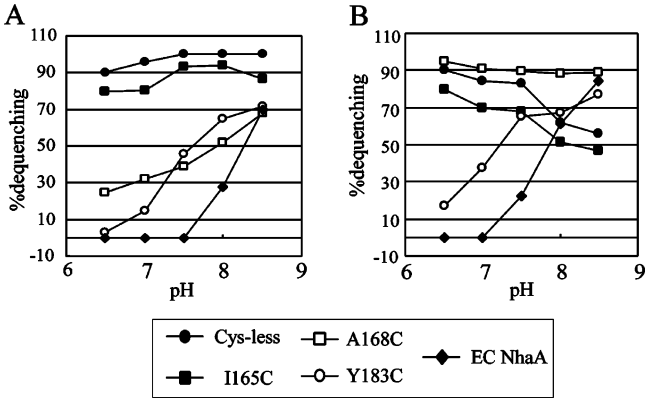

FIGURE 7: Changes in pH dependence of antiporter activity in the Cys-less and Cys mutant NhaAs. Everted membrane vesicles were prepared from KNabc transformants of Cys-less HP NhaA, Cys mutant HP NhaAs, and EC NhaA. Antiporter activities were determined as described in Materials and Methods. The percent fluorescence dequenching observed after the addition of 5 mM NaCl or LiCl is plotted against the pH of the assay. (A) Na^+/H^+ antiporter activity. (B) Li^+/H^+ antiporter activity. Cys-less HP NhaA, (●); I165C, (■); A168C, (□); Y183C, (○); EC NhaA, (♦).

H^+ antiport at acidic pH that is specific to HP NhaA. To our surprise, the Li^+/H^+ antiporter activity for the A168C mutant was similar to the Cys-less control. We have previously reported that Na^+ and Li^+ binding involves different structures (*17*, *19*, *39*), and these data are consistent with the A168C mutation affecting Na^+ but not Li^+ binding.

DISCUSSION

We found that the Cys replacement of several residues in TM5, V162C, A168C, D171C, D172C, and Y183C caused a decrease in antiporter activity. The D171C and D172C mutations, in particular, caused complete loss of activity. These results are consistent with a previously reported random mutation study of HP NhaA (*18*) and a previous analysis of the two corresponding Asp residues of EC NhaA (*12*, *13*), in which the replacement of Asp by Asn completely abrogated antiporter activity. These results, thus, confirm that these Asp residues function as ion binding sites. The replacement of Asp by Cys may cause a conformational change leading to the loss of activity. However, the replacement of these two Asp residues in EC NhaA by 19 other amino acids also caused total loss of activity (Inoue, H., Noumi, T., and Kanazawa, H., unpublished observations), suggesting that the loss of activity is due to the change in the side chain rather than a subsequent conformational change. We showed previously that Asp-141 and Thr-140 in TM4 may be involved in Na^+ or Li^+ binding (*19*). Because Asp-171 and Asp-172 are thought to be involved in H^+ binding, these four residues, Asp-171, Asp-172, Asp-141, and Thr-140, may form the ion binding sites in the antiport process. These residues are in close proximity in the EC NhaA crystal structure (*20*), which is consistent with this hypothesis.

The A168C and Y183C mutations caused an apparent decrease in affinity for the transported ions (Table 1), suggesting that these residues are also involved in ion binding. Interestingly, the A168C and Y183C mutations caused a shift in the pH dependence of the antiporter activity to a range similar to that of EC NhaA (Figure 7). These results suggest that Ala-168 and Tyr-183 are involved in the

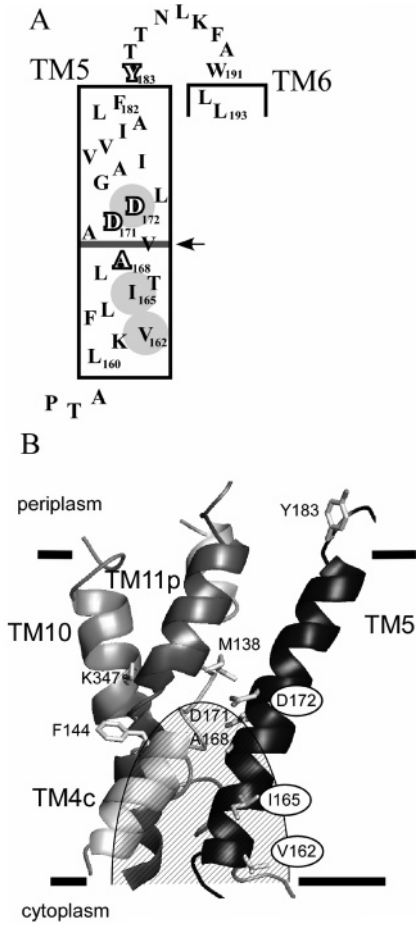

FIGURE 8: Schematic diagrams of TM5 and associated domains. (A) TM5 comprises 23 residues from Leu-160 to Phe-182, as estimated by NEM accessibility experiments. In TM5, the residues facing a water filled channel are shaded. Important residues for ion transport are shown with white letters. A possible boundary between cytoplasmic and periplasmic cavities is indicated by the arrow and the lateral line between Asp-172 and Ile-165. (B) Model structure of TM4, 5, 10, and 11, generated by homology modeling based on the crystal structure of EC NhaA (pdb code, 1ZCD), showing functionally important residues (Phe-144, Met-138, Ala-168, Asp-171, Asp-172, Tyr-183, and Lys-347) and residues located in the hydrophilic environment (circled residues) (*18*, *42*). The EC NhaA crystal structure shows that TM4, TM5, TM2, and TM9 form a water filled cavity open to the cytoplasmic side (*20*). The parts of TM4 and TM5 shown within a shaded area face this cavity. Parts of TM2 and TM9, which are not shown here, form the front side of this cavity. Solid black lines represent the boundary of the membrane indicated by [^{14}C]NEM binding experiments (Figure 3).

acidic pH antiporter activity specific to HP NhaA. However, Ala-168 and Tyr-183 are conserved between EC NhaA and HP NhaA. Thus, these residues alone cannot determine the HP NhaA specific acidic pH antiporter activity, and additional residues may contribute to this activity. One possibility is that Ala-168 and Tyr-183 are functionally associated with Asp-171 and Asp-172, possibly forming a H^+-binding site. Ala-168 is located in the hydrophobic environment and the boundary between the two cavities, which open to the cytoplasm or the periplasm (Figure 8A). Moreover, Ile-165, Ala-168, Asp-171, and Asp-172 seem to be located on the same surface of an α-helix according to the helical wheel model and the EC NhaA crystal structure (Figures 4 and 8B). A recent multiconformation continuum electrostatic analysis based on the crystal structure of EC NhaA showed

that Tyr-183 (Tyr-175 in EC) is involved in a cluster composed of electrostatically interacting residues, including Asp-141 (Asp-133), Asp-171 (Asp-163), Asp-172 (Asp-164), and Lys-347 (Lys-300) (*40*). We reported previously that the M138K and F144L mutations in TM4 as well as K347N in TM10 decreased the antiporter activity at acidic pH (*18*), similar to the A168C and Y183C mutations examined here. Therefore, these three residues are also involved in the antiporter activity at acidic pH. On the basis of our study, together with the multiconformation continuum electrostatic analysis results, we concluded that the proper conformation of the α-helical structure of TM5, which depends on residues, including Ala-168, Tyr-183, Met-138, Phe-144 and Lys-347, may influence the pK_a of Asp-171 and Asp-172. The α-helical structure of TM5 defined by these residues may specify the different pH dependencies between the *E. coli* and *H. pylori* proteins. *H. pylori* lives in acidic conditions in the stomach and is pathogenic for stomach ulcers and cancer (*41*), and the structures involved in the *H. pylori* specific antiporter activity may provide a target for drug treatments to reduce the antiporter activity. This reduction of NhaA activity might lead to the modulation of cell growth of *H. pylori* in the stomach.

NEM labeling experiments revealed that TM5 is comprises 23 residues (Leu-160 to Phe-182), and three residues, Val-162, Ile-165, and Asp-172, are exposed to an aqueous environment. In addition to TM5, loop 5 between TM5 and TM6 consists of residues 183 to 191. On the basis of an α-helical wheel model of the transmembrane region (Figure 4A), three residues, Val-162, Ile-165, and Asp-172, are predicted to be on the same face of the α-helix, suggesting that this face lines the aqueous cavity conducting ion transport. The crystal structure of EC NhaA (*20*) (Figures 4B and 8B) showed that a water filled cavity open to the cytoplasmic side is formed by the parts of TM4, TM5, TM2, and TM9. Val-162 (Ile-154 in EC) and Ile-165 (Met-157), and possibly Asp-172 (Asp-164) face this cavity, consistent with our prediction for these residues of HP NhaA. NEM reacts with D172C but not with D171C, indicating that these two aspartate residues are in different environments. The orientation of the side chains of two Asp residues in EC NhaA crystal structure (Figure 8B) supports this result.

The effect of the membrane impermeable thiol-reactive reagent AMS on NEM binding to V162C and I165C suggests that a water filled channel lined by Val-162 and Ile-165 exists and possibly opens to the cytoplasm. The crystal structure of EC NhaA (*20*) also supports this model, rather than the alternative, that these residues are exposed to an occluded aqueous compartment not exposed to either surface. Inhibition of NEM binding to D172C by pretreatment of intact cells with AMS was not observed, which suggests that Asp-172 faces the aqueous environment on the cytoplasmic side of the membrane. However, pretreatment of intact cells with Ag^+ caused the inhibition of NEM binding, indicating that Ag^+ can access D172C from the periplasmic side of the membrane. This result suggests that a hydrophilic cavity, possibly with Asp-172 located at the end, extends to the periplasmic space but not to the cytoplasmic side. TM5 could, thus, be involved in the formation of two different water filled cavities, one open to the cytoplasm and the other open to the periplasm. In the presence of AMS, reactivity to NEM was increased for I165C and D172C (Figure 6). Because AMS binds to Cys residues on the membrane surface, its presence may lead to a relative increase in free NEM.

Because Asp-171 and Asp-172 are located in hydrophobic and hydrophilic environments, respectively, a putative hydrophobic barrier seems to be located at Asp-171 and/or close to residues between Ile-165 and Asp-172 (Figure 8A). Although the structural characteristics of a putative hydrophobic barrier are not precisely defined at present, it is highly probable that this putative hydrophobic barrier may function as a gate between the two water filled cavities. These two cavities and the putative gate structure may form an hourglass-like structure. Because Asp-171 is essential for antiporter activity, Asp-171 may not always be in a hydrophobic environment that is not NEM reactive. Therefore, we believe that alternating proton binding to both Asp-171 and Asp-172 occurs during the operation of the antiporter. Proton binding to one of these residues might cause a local conformational change, leading to a transient reduction in the hydrophobic barrier and translocation of the ions. This assumption could be an important clue for future experimental studies to detect conformational changes in the putative gate, which are required for ion translocation. The topology of Asp-172 identified in this study is inconsistent with the crystal structure of EC NhaA, in which Asp-172 (Asp-164 in EC NhaA) is exposed to the cytoplasmic space. The apparent difference in topology of the two Asp's from HP and EC NhaA could also reflect active and inactive states of the gate area. NEM binding to D172C was inhibited by Ag^+ but not by AMS. This difference may be due to differences in the size of the two inhibitors and suggests that Asp-172 is probably located in a narrower hydrophilic space that Ag^+ but not AMS is able to enter.

Multiple conformational changes may occur during the antiport in NhaA. In the present study, we labeled NhaA with NEM in the absence of Na^+ or Li^+ at pH 7. Therefore, the structure we predict here may reflect one of several expected conformations. NEM labeling in the presence of various concentrations of Na^+ or Li^+ will provide additional information about the putative conformations of the transporter.

REFERENCES

1. Padan, E., and Schuldiner, S. (1992) *Alkali Cation Transport Systems in Procaryotes* (Bakker, E., Ed.) pp 3−24, CRC Press, Inc., Boca Raton, FL.
2. Padan, E., and Schuldiner, S. (1994) Molecular physiology of Na^+/H^+ antiporters, key transporters in circulation of Na^+ and H^+ in cells, *Biochim. Biophys. Acta. 1185*, 129−151.
3. Schuldiner, S., and Padan, E. (1992) *Alkali Cation Transport Systems in Procaryotes* (Bakker, E., Ed.) pp 25−51, CRC Press, Inc., Boca Raton, FL.
4. Padan, E. (1998) *Microbiology and Biochemistry of Hypersaline Environments* (Oren, A., Ed.) pp 163−175, CRC Press, Inc., Boca Raton, FL.
5. Karpel, R., Olami, Y., Taglicht, D., Schuldiner, S., and Padan, E. (1988) Sequencing of the gene *ant* which affects the Na^+/H^+ antiporter activity in *Escherichia coli*, *J. Biol. Chem. 263*, 10408−10414.
6. Pinner, E., Padan, E., and Schuldiner, S. (1992) Cloning, sequencing, and expression of the *nhaB* gene, encoding a Na^+/H^+ antiporter in *Escherichia coli*, *J. Biol. Chem. 267*, 11064−11068.
7. Ivey, D. M., Guffanti, A. A., Zemsky, J., Pinner, E., Karpel, R., Padan, E., Schuldiner, S., and Krulwich, T. A. (1993) Cloning and characterization of a putative Ca^{2+}/H^+ antiporter gene from Escherichia coli upon functional complementation of Na^+/H^+ antiporter- deficient strains by the overexpressed gene, *J. Biol. Chem. 268*, 11296−11303.

8. Taglicht, D., Padan, E., and Schuldiner, S. (1991) Overproduction and purification of a functional Na^+/H^+ antiporter coded by *nhaA* (*ant*) from *Escherichia coli*, *J. Biol. Chem. 266*, 11289−11294.
9. Pinner, E., Padan, E., and Schuldiner, S. (1994) Kinetic properties of NhaB, a Na^+/H^+ antiporter from *Escherichia coli*, *J. Biol. Chem. 269*, 26274−26279.
10. Rothman, A., Padan, E., and Schuldiner, S. (1996) Topological analysis of NhaA, a Na^+/H^+ antiporter from *Escherichia coli*, *J. Biol. Chem. 271*, 32288−32292.
11. Williams, K. A. (2000) Three-dimensional structure of the ion-coupled transport protein NhaA, *Nature 403*, 112−115.
12. Inoue, H., Noumi, T., Tsuchiya, T., and Kanazawa, H. (1995) Essential aspartic acid residues, Asp-133, Asp-163 and Asp-164, in the transmembrane helices of a Na^+/H^+ antiporter (NhaA) from *Escherichia coli*, *FEBS Lett. 363*, 264−268.
13. Noumi, T., Inoue, H., Sakurai, T., Tsuchiya, T., and Kanazawa, H. (1997) Identification and characterization of functional residues in a Na^+/H^+ antiporter (NhaA) from *Escherichia coli* by random mutagenesis, *J. Biochem. (Tokyo) 121*, 661−670.
14. Gerchman, Y., Olami, Y., Rimon, A., Taglicht, D., Schuldiner, S., and Padan, E. (1993) Histidine-226 is part of the pH sensor of NhaA, a Na^+/H^+ antiporter in *Escherichia coli*, *Proc. Natl. Acad. Sci. U.S.A. 90*, 1212−1216.
15. Rimon, A., Gerchman, Y., Kariv, Z., and Padan, E. (1998) A point mutation (G338S) and its suppressor mutations affect both the pH response of the NhaA-Na^+/H^+ antiporter as well as the growth phenotype of *Escherichia coli*, *J. Biol. Chem. 273*, 26470−26476.
16. Inoue, H., Sakurai, T., Ujike, S., Tsuchiya, T., Murakami, H., and Kanazawa, H. (1999) Expression of functional Na^+/H^+ antiporters of *Helicobacter pylori* in antiporter-deficient *Escherichia coli* mutants, *FEBS Lett. 443*, 11−16.
17. Inoue, H., Tsuboi, Y., and Kanazawa, H. (2001) Chimeric Na^+/H^+ antiporters constructed from NhaA of *Helicobacter pylori* and *Escherichia coli*: Implications for domains of NhaA for pH sensing, *J. Biochem. (Tokyo) 129*, 569−576.
18. Tsuboi, Y., Inoue, H., Nakamura, N., and Kanazawa, H. (2003) Identification of membrane domains of the Na^+/H^+ antiporter (NhaA) protein from *Helicobacter pylori* required for ion transport and pH sensing, *J. Biol. Chem. 278*, 21467−21473.
19. Kuwabara, N., Inoue, H., Tsuboi, Y., Nakamura, N., and Kanazawa, H. (2004) The fourth transmembrane domain of the *Helicobacter pylori* Na^+/H^+ antiporter NhaA faces a water-filled channel required for ion transport, *J. Biol. Chem. 279*, 40567−40575.
20. Hunte, C., Screpanti, E., Venturi, M., Rimon, A., Padan, E., and Michel, H. (2005) Structure of a Na^+/H^+ antiporter and insights into mechanism of action and regulation by pH, *Nature 435*, 1197−1202.
21. Brewer, C. F., and Riehm, J. P. (1967) Evidence for possible nonspecific reactions between *N*-ethylmaleimide and proteins, *Anal. Biochem. 18*, 248−255.
22. Nozaki, K., Inaba, K., Kuroda, T., Tsuda, M., and Tsuchiya, T. (1996) Cloning and sequencing of the gene for Na^+/H^+ antiporter of *Vibrio parahaemolyticus*, *Biochem. Biophys. Res. Commun. 222*, 774−779.
23. Messing, J., and Vieira, J. (1982) A new pair of M13 vectors for selecting either DNA strand of double-digest restriction fragments, *Gene 19*, 269−276.
24. Kanazawa, H., Miki, T., Tamura, F., Yura, T., and Futai, M. (1979) Specialized transducing phage lamda carrying the genes for coupling factor of oxidative phosphorylation of *Escherichia coli*: Increased synthesis of coupling factor on induction of prophage lamda asn, *Proc. Natl. Acad. Sci. U.S.A. 76*, 1126−1130.
25. Inoue, H., Noumi, T., Shimomura, T., Takimoto, N., Tsuchiya, T., and Kanazawa, H. (1998) pH-dependent growth retardation of *Escherichia coli* caused by overproduction of Na^+/H^+ antiporter, *Biol. Pharm. Bull. 21*, 1128−1133.
26. Hashimoto-Gotoh, T., Mizuno, T., Ogasahara, Y., and Nakagawa, M. (1995) An oligodeoxyribonucleotide-directed dual amber method for site-directed mutagenesis, *Gene 152*, 271−275.
27. Miki, J., Kusuki, K., Tsugumi, H., and Kanazawa, H. (1994) Amino acid replacements at binding sites of monoclonal antibody in the F_1-ATPase beta subunit from *Escherichia coli* caused altered subunit interactions, *J. Biol. Chem. 269*, 4227−4232.
28. Rosen, B. (1986) Recent advances in bacterial ion transport, *Annu. Rev. Microbiol. 40*, 263−286.
29. Goldberg, E. B., Arbel, T., Chen, J., Karpel, R., Mackie, G. A., Schuldiner, S., and Padan, E. (1987) Characterization of a Na^+/H^+ antiporter gene of *Escherichia coli*, *Proc. Natl. Acad. Sci. U.S.A. 84*, 2615−2619.
30. Rosen, B. (1986) Ion extrusion systems in *Escherichia coli*, *Methods Enzymol. 125*, 328−336.
31. Schuldiner, S., and Fishkes, H. (1978) Sodium-proton antiport in isolated membrane vesicles of *Escherichia coli*, *Biochemistry 17*, 706−710.
32. Laemmli, U. K. (1970) Cleavage of structural proteins during the assembly of the head of bacteriophage T4, *Nature 227*, 680−685.
33. Maniatis, T., Fritsch, E. F., and Sambrook, J. (1982) *Molecular Cloning: A Laboratory Manual*, Cold Spring Harbor Laboratory, Cold Spring Harbor, NY.
34. Lowry, O. H., Rosebrough, N. J., Farr, A. L., and Randall, R. J. (1951) Protein measurement with the folin phenol reagent, *J. Biol. Chem. 193*, 265−275.
35. Yan, R. T., and Maloney, P. C. (1995) Residues in the pathway through a membrane transporter, *Proc. Natl. Acad. Sci. U.S.A. 92*, 5973−5976.
36. Frillingos, S., Sahin-Toth, M., Wu, J., and Kaback, H. R. (1998) Cys-scanning mutagenesis: a novel approach to structure−function relationships in polytopic membrane proteins, *FASEB J. 12*, 1281−1299.
37. Kimura-Someya, T., Iwaki, S., and Yamaguchi, A. (1998) Site-directed chemical modification of cysteine-scanning mutants as to transmembrane segment II and its flanking regions of the Tn*10*-encoded metal-tetracycline/H^+ antiporter reveals a transmembrane water-filled channel, *J. Biol. Chem. 273*, 32806−32811.
38. Kuroda, T., Shimamoto, T., Inaba, K., Tsuda, M., and Tsuchiya, T. (1994) Properties and sequence of the NhaA Na^+/H^+ antiporter of *Vibrio parahaemolyticus*, *J. Biochem. (Tokyo) 116*, 1030−1038.
39. Karasawa, A., Tsuboi, Y., Inoue, H., Kinoshita, R., Nakamura, N., and Kanazawa, H. (2005) Detection of oligomerization and conformational changes in the Na^+/H^+ antiporter from *Helicobacter pylori* by fluorescence resonance energy transfer, *J. Biol. Chem. 280*, 41900−41911.
40. Olkhova, E., Hunte, C., Screpanti, E., Padan, E., Michel, H. (2006) Multiconformation continuum electrostatics analysis of the NhaA Na^+/H^+ antiporter of *Escherichia coli* with functional implications. *Proc. Natl. Acad. Sci. U.S.A. 103*, 2629−2634.
41. van Amsterdam, K., van Vliet, A. H., Kusters, J. G., and van der Ende, A. (2006) Of microbe and man: determinants of *Helicobacter pylori*-related diseases, *FEMS Microbiol. Rev. 30*, 131−156.
42. Lund, O., Nielsen, M., Lundegaard, C., and Worning, P. (2002) CPHmodels 2.0: X3M a computer program to extract 3D models. *Abstract of the CASP5 Conference*, A 102.

BI061048D